



## Prediction of Ozone Concentrations over the Sea of Japan Coastal Area Using WRF/Chem Model

*Khandakar Md Habib Al Razi and Moritomi Hiroshi*

Environmental and Renewable Energy System (ERES),  
Graduate School of Engineering, Gifu University, Yanagido, Gifu City, Japan

(Received: December 28, 2011; Accepted: January 30, 2012)

**Abstract:** The fully coupled WRF/Chem (Weather Research and Forecasting/Chemistry) model is used to simulate air quality over the Sea of Japan coastal area. Anthropogenic surface emissions database used as input for this model are mainly based on Global hourly emissions data (dust, sea salt, biomass burning), RETRO (REanalysis of the TROpospheric chemical composition), GEIA (Global Emissions Inventory Activity) and POET (Precursors of ozone and their Effects in the Troposphere). Climatologic concentrations of particulate matters derived from Regional acid Deposition Model (RADM2) chemical mechanism and Secondary Organic Aerosol Model (MADE/SORGAM) with aqueous reaction were used to deduce the corresponding aerosols fluxes for input to the WRF/Chem. The model was firstly integrated for 48 hours continuously starting from 00:00 UTC of 14 March 2008 to evaluate ozone concentrations and other precursor pollutants were analyzed. WPS meteorological data were used for the simulation of WRF/Chem model in this study. Despite the low resolution of the area global emissions and the weak density of the local point emissions, it has been found that WRF/Chem simulates quite well with the diurnal variation of the chemical species concentrations over the Sea of Japan coastal area. The simulations conducted in this study showed that due to the geographical and climatologically characteristics, it is still environmentally friendly by the transported pollutants in this region.

**Key words:** Air quality; Modeling; WRF/Chem; Ozone concentrations

### INTRODUCTION

At the present, more than 60 million people are added to cities each year worldwide, about 325 cities have a population of more than one million, compared to 270 in 1990 [1]. In recent decades, air quality has deteriorated remarkably in the large cities of the developing countries. The export of air pollutants from urban to regional and global environments is of major concern because of wide-ranging potential consequences for human health and for cultivated and natural ecosystems, visibility degradation, weather modification, radiative forcing and changes in tropospheric oxidation (self-cleaning) capacity. Rapidly increasing urbanization will be a major environmental driving force in the 21st century, affecting air quality on

all scales-local, regional and global [1]. Large numbers of people are likely to be exposed to unhealthy ozone concentrations when ground-level ozone accumulates in urban metropolitan areas under certain weather conditions [2] and quantitative atmospheric dispersion models will be of great help to provide effective decision support systems for planners and administrators.

The main pollutants emitted into the atmosphere in urban area are sulfur oxides ( $\text{SO}_x$ ), nitrogen oxides ( $\text{NO}_x$ ), carbon monoxide (CO), volatile organic compounds (VOCs), metal oxides and particular matter (PM/aerosols) mostly consisting of black carbon, sulfates, nitrates and organic matter. The oxidizations of CO, VOCs and  $\text{NO}_x$  produce  $\text{O}_3$  in the PBL (Planetary Boundary Layer) which has important impact on human's health in urban area.

The recent economical developments of Korea and Japan are very rapid due to rapid growth of heavy industrial operations. The rapid growing urbanization will cause wide-ranging potential consequences for environmental problems. These areas have been suffering server air pollution problems, such as high particular matter (PM) concentrations and poor visibility [3-6]. As the increase in industrial activity and number of automobiles, the emission of VOCs (volatile organic carbons) and NO<sub>x</sub> (NO + NO<sub>2</sub>) will be significantly increased. Both VOCs and NO<sub>x</sub> play critical roles in O<sub>3</sub> formation in the troposphere [7, 8] and the variations in their concentrations and the ensuing effects on O<sub>3</sub> production rate can be characterized as either NO<sub>x</sub>-sensitive or VOC-sensitive [7, 9-12]. Thus, better understanding the relationship between O<sub>3</sub> precursors (VOCs, NO<sub>x</sub>) and O<sub>3</sub> formation in East Asia is one of the critical pre-required information to develop effective O<sub>3</sub> control strategies [13-15].

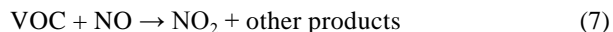
In Japan, VOC, NO<sub>x</sub> and SO<sub>x</sub> categorized as a hazardous air pollutant (HAP) in 1996 and are on the list of Substances Requiring Priority Action published by the Central Environmental Council of Japan [16]. The Central Environmental Council made the second report on "Future direction of measures against hazardous air pollutants" in Oct. 1996. The second report also proposed that the voluntary action to reduce emission, as well as investigation of hazardousness, atmospheric concentrations and pollution source of those substances should be promoted. Although the industrial emission of VOC, NO<sub>x</sub> and SO<sub>x</sub> in Japan have been decreased in recent years, primarily due to voluntary reductions from industrial sources, the risks of exposure to this pollutant have remained largely unknown. In this study, a rapid change of O<sub>3</sub> and its precursors are simulated during the spring and summer time in 2008. The simulation result leads to better understanding O<sub>3</sub> variability in the Sea of Japan coastal area [17]. A three dimensional chemical/dynamical regional model (WRF/Chem V-3.3) is applied to analyze the causes of the rapid changes of O<sub>3</sub> during this period.

Ozone (O<sub>3</sub>) is not emitted directly into the air; instead it forms in the atmosphere as a result of a series of complex chemical reactions between oxides of nitrogen (NO<sub>x</sub>) and hydrocarbons, which together are precursors of ozone. Ozone precursors have both anthropogenic (man-made) and biogenic (natural) origins. Motor vehicle exhaust, industrial emissions, gasoline vapors and chemical solvents are some of the major sources of NO<sub>x</sub> and hydrocarbons. Many species of vegetation including trees and plants emit hydrocarbons and fertilized soils release NO<sub>x</sub>.

In the presence of ultraviolet radiation (*hν*), oxygen (O<sub>2</sub>) and nitrogen dioxide (NO<sub>2</sub>) react in the atmosphere to form ozone and nitric oxide (NO) [18, 19]. The resultant ozone reacts with NO to form nitrogen dioxide. A steady state is attained through these reactions:



Even without anthropogenic emissions, these reactions normally result in a natural background ozone concentrations of 25 to 45 ppb [20, 21]. Ozone cannot accumulate further unless volatile organic compounds (VOCs), which include hydrocarbons, are present to consume or convert NO back to NO<sub>2</sub> [19, 22, 23] as:



This equation is a simplified version of many complex chemical reactions. As NO is consumed by this process, it is no longer available to react with ozone. When additional VOCs are added to the atmosphere, a greater proportion of the NO is oxidized to NO<sub>2</sub>, resulting in greater ozone formation. Anthropogenic sources of NO lead to higher levels of NO<sub>2</sub> in the atmosphere, which will be available for photolysis. The formation and increase in ozone concentrations occur over a period of a few hours. Shortly after sunrise, NO and VOCs react in sunlight to form ozone. Throughout the morning, ozone concentrations increase while NO and VOCs are depleted. Eventually, either the lack of sunlight, NO, or VOCs limit the production of ozone. This diurnal cycle varies greatly depending on site location, emission sources and weather conditions. Precursor emissions of NO and VOC are necessary for ozone to form in the troposphere. Understanding the nature of when and where ozone precursors originate may help forecasters to factor day-to-day emissions changes. For example, if a region's emissions are dominated by mobile sources, emissions and hence the ozone that forms may depend on the day-of-week commute patterns. The dominant NO<sub>x</sub> producers are combustion processes, including industrial and electrical generation processes and mobile sources such as automobiles. Mobile sources also account for a large portion of VOC emissions. Industries such as the chemical industry or others that use solvents also account for a large portion of VOC emissions. Biogenic VOC emissions

from forested and vegetative areas may impact urban ozone formation in some parts of the country. Biogenic NO<sub>x</sub> emissions levels are typically much lower than anthropogenic NO<sub>x</sub> emissions levels. [24].

In this present study, a preliminary evaluation of the model performance by comparison to the online observation obtained from different monitoring stations at the past year in Japan. The spatial and temporal dynamics was studied using simulations performed with the Weather Research and Forecast (WRF) model [25] coupled with Chemistry (WRF/Chem) [26]. Due to the geographical complexity of the area the important part of the study was also the evaluated of the model's ability to represent the measured meteorological conditions and surface ozone levels.

**Model Description:** The weather research and forecasting (WRF) model is a mesoscale numerical weather prediction system designed to serve both operational forecasting and atmospheric research needs. The effort to develop WRF has been a collaborative partnership, principally among the National Center for Atmospheric Research (NCAR), the National Oceanic and Atmospheric Administration (NOAA), the National Center for Environmental Prediction (NCEP), the Forecast Systems Laboratory (FSL), the Air Force Weather Agency (AFWA), the Naval Research Laboratory, Oklahoma University and the Federal Aviation Administration (FAA). The WRF model is a fully compressible and Euler nonhydrostatic model. It calculates winds (*u*, *v* and *w*), perturbation potential temperature, perturbation geopotential and perturbation surface pressure of dry air. It also can optionally output other variables, including turbulent kinetic energy, water vapor mixing ratio, rain/snow mixing ratio and cloud water/ice mixing ratio. The model physics include bulk schemes, mixed-phase physics for cloud-resolving modeling, multi-layer land surface models ranging from a simple thermal model to full vegetation and soil moisture models, including snow cover and sea ice, turbulent kinetic energy prediction or non-local K schemes for planetary boundary layer calculation and longwave and shortwave schemes with multiple spectral bands and a simple shortwave scheme. A detailed description of the WRF model can be found on the WRF web-site <http://www.wrf-model.org/index.php>.

In addition to a dynamical calculation, a chemical model (WRF/Chem) is fully (on-line) coupled with the WRF model. A detailed description of WRF/Chem is given by Grell *et al.* [26]. The version of the model (Version-3.3), as used in the present study, includes simultaneous calculation of dynamical parameters

(winds, temperature, boundary layer, clouds, etc.), transport (advective, convective and diffusive), dry deposition [27], gas phase chemistry, radiation and photolysis rates [28, 29] and surface emissions, including online calculation of biogenic emission. Ozone chemistry is represented in the model by a modified Regional Acid Deposition Model, version 2 (RADM2) gas phase chemical mechanism [30] which includes 158 reactions among 36 species with Secondary Organic Aerosol Model (MADE/SORGAM) of aqueous reaction [31].

### **Method of Simulation**

**Model Settings:** The Sea of Japan coastal area considered in the present study were located (latitude 31.4 - 45.0 N and longitude 129.3 - 146.2 E), which is a marginal sea of the western Pacific Ocean, bordered by Japan, Korean peninsula and Russia and is referred to in South Korea as the East Sea [32, 33].

In this study, the model is used to simulate medium scale and regional circulations influenced by the complex terrain within and around the Sea of Japan coastal area during the period 00:00 UTC (Coordinated Universal Time) [34] of 14 March 2008 to 00.00 of 16 March 2008, whereas Japan Standard Time (JST) [35] is the standard time zone of Japan and is 9 hours ahead of UTC. One nesting domains was defined using Lambert projection, which can be seen in Figure 1. The domain covers the Sea of Japan coastal area with the center point of 38.5°N, 137.60°E, horizontal grids of 75 × 70 and grid spacing of 22 km. The domain settings and configuration options are shown in Table 1. The initial meteorological fields and boundary conditions are from NCEP global reanalysis data with a horizontal resolution of 0.5° by 0.5° and 35 vertical levels, non-uniformly spaced, from the surface to 20 mbar. The boundary conditions were forced every 6 hours. The ideal concentrations profiles [36] were used as initial and boundary conditions of chemical species.

**Emissions Data Acquisition and Pre-processing:** The linkages in the formation and transport of pollution between the local, regional and global scales are receiving increasing recognition and a variety of atmospheric chemistry models address these aspects. This puts new demand on the emission inventories that are used as input to these models. They need to be accurate at the local scale yet cover the entire globe with a consistent approach.

The GEIA (Global Emissions Inventory Activity) / ACCENT (European Network of Excellence on Atmospheric Composition Change) data portal is a cooperative effort providing surface emissions data

Table 1: WRF/Chem domain setting and configuration options

Horizontal grid (x,y)	75, 70
Grid spacing	22 km
Meteorological time step	180 s
Chemical time step	180 s
Microphysics	WSM3-class simple ice scheme [59]
Advection scheme	5th horizontal/3rd vertical [60, 61]
Long-wave radiation	RRTM [62]
Short-wave radiation	GODDARD [63, 64]
Surface layer	Moni-Obukhov (Janjic Eta) [65]
Land-surface model	NOAH [66]
Boundary layer	Mellor-Yamada-Janjic TKE [67, 68]
Cumulus parameterization	Grell-Devenyi ensemble scheme [69]
Chemistry option	RADM2 [70]
Dry deposition	Wesley, 1989 [71]
Biogenic emissions	Guenther scheme [72, 73]
Photolysis option	Madronich, 1987 [74]
Aerosol option	MADE/SORGAM [75]

Table 2: Global inventories offered by the GEIA/ACCENT data portal

Inventory	Categories	Spatial resolution	Temporal resolution
POET [76, 77]	Anthropogenic biomass burning (natural)	1° x 1°	Annual (anthro.) monthly (biom. burn.) monthly (natural)
RETRO [78]	Anthropogenic biomass burning	0.5° x 0.5°	Monthly
EDGAR	Anthropogenic biomass burning	1° x 1°	Annual
GFED v2 [82, 83]	Biomass burning	1° x 1°	Monthly 8 day (available: <a href="http://daac.ornl.gov/VEGETATION/guides/global_fire_emissions_v2.1.html">http://daac.ornl.gov/VEGETATION/guides/global_fire_emissions_v2.1.html</a> )
CO <sub>2</sub> [84]	Anthropogenic	1° x 1°	Annual
GEIA v.1 [80]	Anthropogenic biomass burning natural	1° x 1°	Annual + monthly for NO <sub>x</sub> , SO <sub>2</sub> and nat.VOC

(total and gridded data), for the main emission categories (total anthropogenic, total biomass burning, biogenic and oceans) at global or regional scales, from several inventories (RETRO, POET, EDGARFT2000, GFEDv2, GEIA v1, etc) (Table 2).

The use of a global emissions data set has recently been added to WRF/Chem options. The global emissions data comes from the Reanalysis of the Tropospheric (RETRO) chemical composition over the past 40 years (<http://retro.enes.org/index.shtml>) and Emission Database for Global Atmospheric Research (EDGAR) (<http://www.mnp.nl/edgar/introduction>). Both RETRO and EDGAR provide global annual emissions for several greenhouse gases (e.g. CO<sub>2</sub>, CH<sub>4</sub> and N<sub>2</sub>O) as well as some precursor gases on a 0.5° x 0.5° (RETRO) or a 1° x 1° (EDGAR) grid. In this present study a simple grid mapping program has been used in the WRF/Chem model. This program, called 'prep\_chem\_sources' for Global emissions data (dust, sea salt, biomass burning), was developed at CPTEC, Brazil and is available to WRF/Chem users. The program will map the global anthropogenic emissions data to a WRF forecast domain using a polar stereographic or Lambert conformal projection.

### Observation of Ozone Concentrations over Japan:

Annual and monthly pollutant concentrations observed at monitoring stations operated by Japanese, local governments and Japan Meteorological Agency [37, 38] (JMA) are available on the website [39]. It contains the monitoring data since 1970, which are valuable to evaluate the long-term or short-term trends of pollutant concentrations in Japan. The increasing trend of surface ozone in Japan has been reported annually by the Japanese government based on this database [40]. Observation data at 1045 monitoring stations which continued monitoring for photo-chemical oxidants during 1996-2005 was noted in this study to know the scenario of ozone concentrations in March and to compare with simulation result. Most of the monitoring stations are located in coastal populated areas in Japan as shown in the left map of Figure 1 because they are operated mainly to evaluate the attainment of environmental quality standard (EQSs). This database has compiled surface ozone concentrations as a daytime average and maximum concentrations of photo-chemical oxidants. Daytime corresponds to thirteen hours from 05:00 a.m. to 06:00 p.m. Photo-chemical oxidants include other trace oxidants like H<sub>2</sub>O<sub>2</sub> and PAN, but instruments which detect only ozone

have been officially approved by the Japanese government because differences in concentrations of photochemical oxidants and ozone are expected to be small [41]. Therefore, differences in concentrations between ozone and photochemical oxidants can be ignored for monthly variation of observed concentrations of surface ozone. Additionally, the Acid Deposition Monitoring Network in East Asia (EANET) operates monitoring stations located mainly in remote areas. Observed concentrations of surface ozone at ten EANET monitoring stations in Japan were used to validate the performance of the simulation in Japanese background areas during 2000-2005. The locations of EANET monitoring stations are shown in the middle map of Figure 2. They are scattered in remote areas throughout Japan.

The concentrations of surface ozone at EANET monitoring stations in Japan shows a seasonal variation with low values in summer (August) and higher value in Spring (April). The average ozone concentrations in march in different EANET monitoring stations were found about 37 ppb to 55 ppb and about 33.5 ppb over Japanese populated areas. Figure 2 shows monthly variations of concentrations of observed surface ozone, averaged during 2000-2005 at each of ten EANET monitoring stations. The red line in Figure 2 shows monthly variations of observed concentrations of surface ozone averaged during 1996-2005 over Japanese populated areas.

### Modeling Results and Discussions

**Ozone Concentration by WRF/Chem Simulation:** Figure 3, which is the composite image from the modeling results of single nesting domains, illustrates the spatial distribution

of surface  $O_3$  concentrations averaged from 00:00 UTC of 14 March (9:00 a.m. of Japanese Standard time) to 00:00 UTC of 16 March of 2008. In order to display the time evolution of the simulated ozone concentrations, Figure 4 shows the structure of the ozone field from 03:00 UTC of March 14 to 00:00 UTC of 16 March of 2008 at 100 meter height above the surface level. This level was chosen in order to emphasize the transport processes across the Sea of Japan coastal area relative to surface processes. The two days simulation shows that Sea of Japan has low to moderate ozone concentrations. The high  $O_3$  concentrations zone was calculated mainly over the Sea of Japan ocean regions during 14 March, whereas the ozone concentrations was calculated 40 to 45 ppb in the Figure 4. At 09:00 UTC of March 14, ozone starts building up in the boundary layer with concentrations of 44 ppb near the Sea of Korean peninsula. An anticyclone [42] moved the high-ozone region rotates anticlockwise from the Sea of Korean peninsula (09:00 UTC of March 14) to the southwest part of the Honshu island of Japan (15:00 UTC of March 14) and then Pacific ocean (06:00 UTC of March 15). Due to the longer life time of  $O_3$  (about a week) in the troposphere, the distribution of  $O_3$  concentrations are greatly influenced by airflow of the anticyclone. Figure 5 shows the clockwise movement of airflow in an anticyclonic rotation at latitude 41.6N, longitude 138.4E at 15:00 UTC of March 14, which moved to the east at 00:00 UTC of March 15 at latitude 42N, longitude 140E. After 00:00 UTC of March 15, maximum ozone concentrations (50 ppb) were found in the south part of the Honshu island of Japan. Another small area of high ozone concentrations built up near the coastal area of the east part of the Honshu island of Japan (00:00 UTC of March

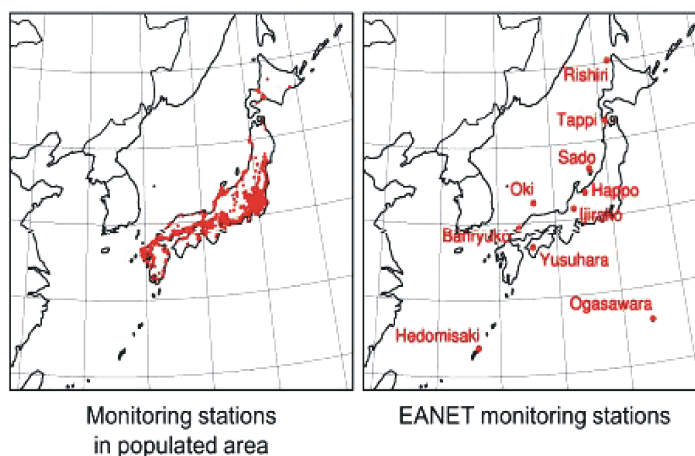


Fig. 1: Location maps of monitoring stations in populated area, and EANET monitoring stations in Japan which were used in this study [41].

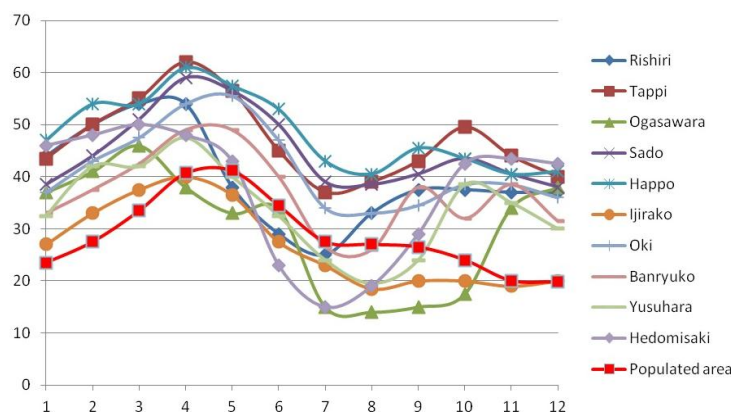


Fig. 2: Monthly variations of observed concentrations of surface ozone, averaged during 2000-2005 at each of ten EANET monitoring stations. The red line shows monthly variations of observed concentrations of surface ozone averaged during 1996-2005 over Japanese populated areas.

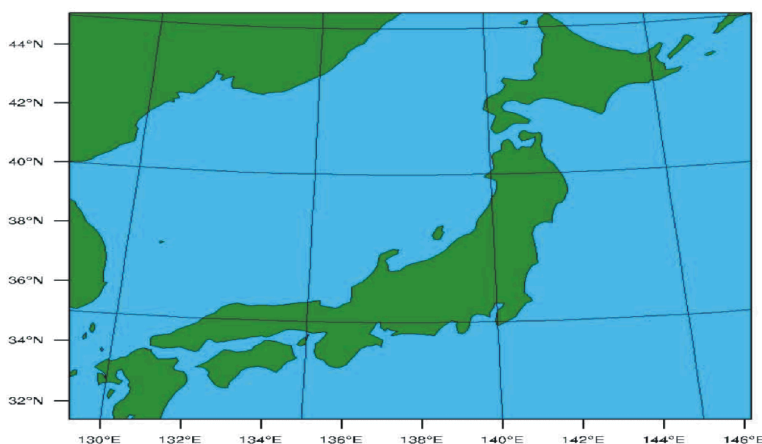


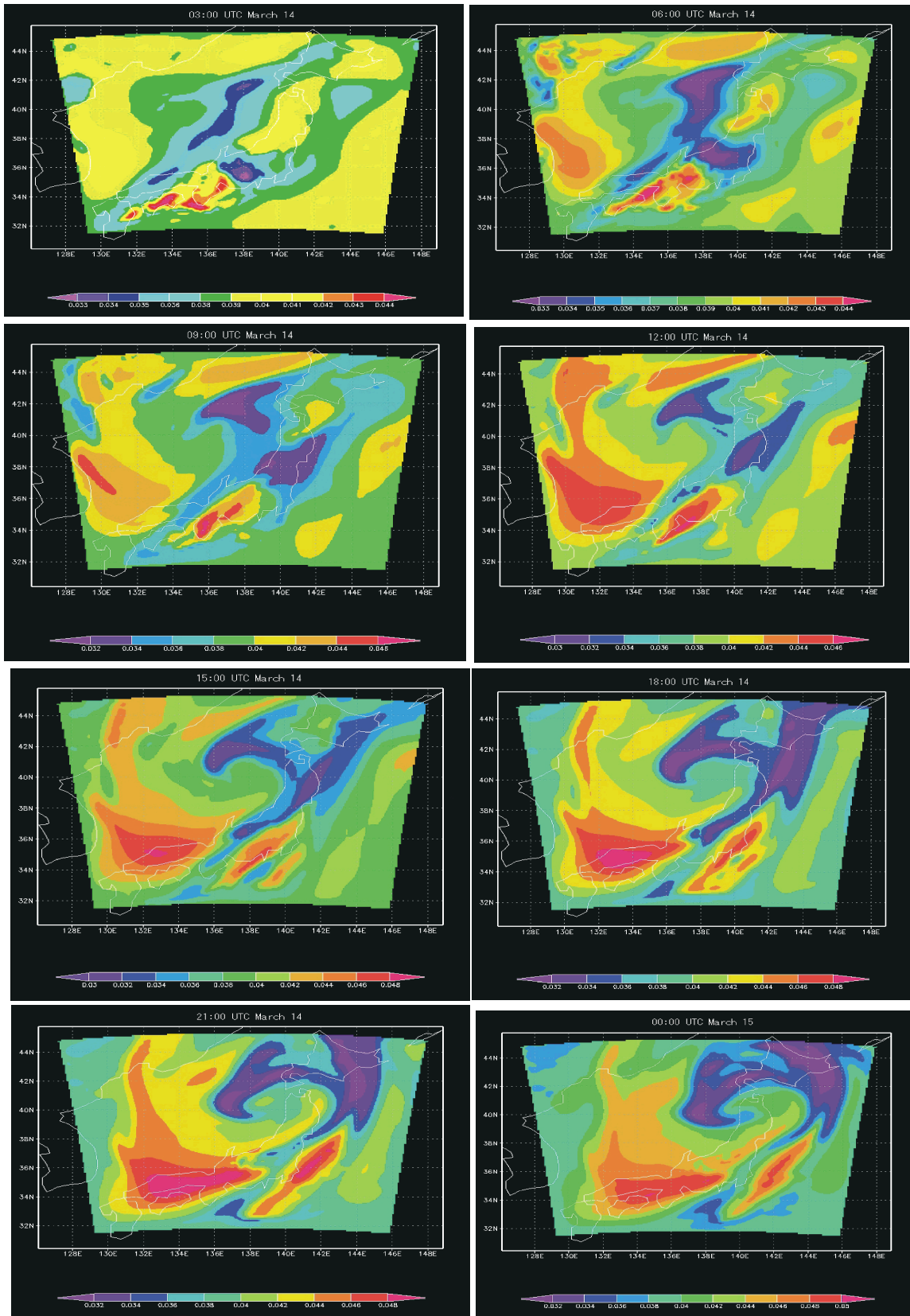
Fig. 3: Nesting domain setting of the model.

14) which stagnated for some hours, then moved to the Pacific ocean, the whole polluted air mass is pushed away eastward by a cold front coming from the northwest [43]. In addition, the level of primary pollutants, such as  $\text{NO}_x$ , were relatively lower over the ocean, resulting in the less consumption of  $\text{O}_3$ , thus the high concentrations of  $\text{O}_3$  are found in ocean. An important fact revealed by the simulated result, ozone levels did not reach extreme values (70-90 ppb) [44].

**Comparison of Simulation Result with Eanet Monitoring**

**Data:** Table 3 shows the accuracy of WRF/Chem simulation result comparing with EANET monitoring data. Though the finer resolution in WRF/Chem effectively titrates ambient ozone and moved the simulated concentrations of surface ozone closer to the observed value, WRF/Chem underestimates surface ozone concentrations in March over the most of the EANET monitoring stations in Japan, Besides WRF/Chem

overestimates the surface ozone concentrations over the Populated area in Japan. Standard deviation was calculated about 6 in EANET monitoring stations comparing with WRF/Chem simulation result, which shows a reasonable agreement with the monitoring data with respect to predicting localized atmospheric ozone concentrations. Absolute values of ozone concentrations are comparable but seasonal variations are different between observed and simulated surface ozone. Therefore, it is complicated to compare the WRF/Chem simulation result of ozone concentration in March with observation data. Concentrations of observed surface ozone are the highest in spring and the lowest in summer at all stations. Second peaks in autumn were found at most of stations. In March the range of observed average ozone concentrations were found about 37.5 ppb to 55 ppb, whereas the average ozone concentrations calculated by WRF/Chem was 40 ppb to 48 ppb in EANET monitoring stations.



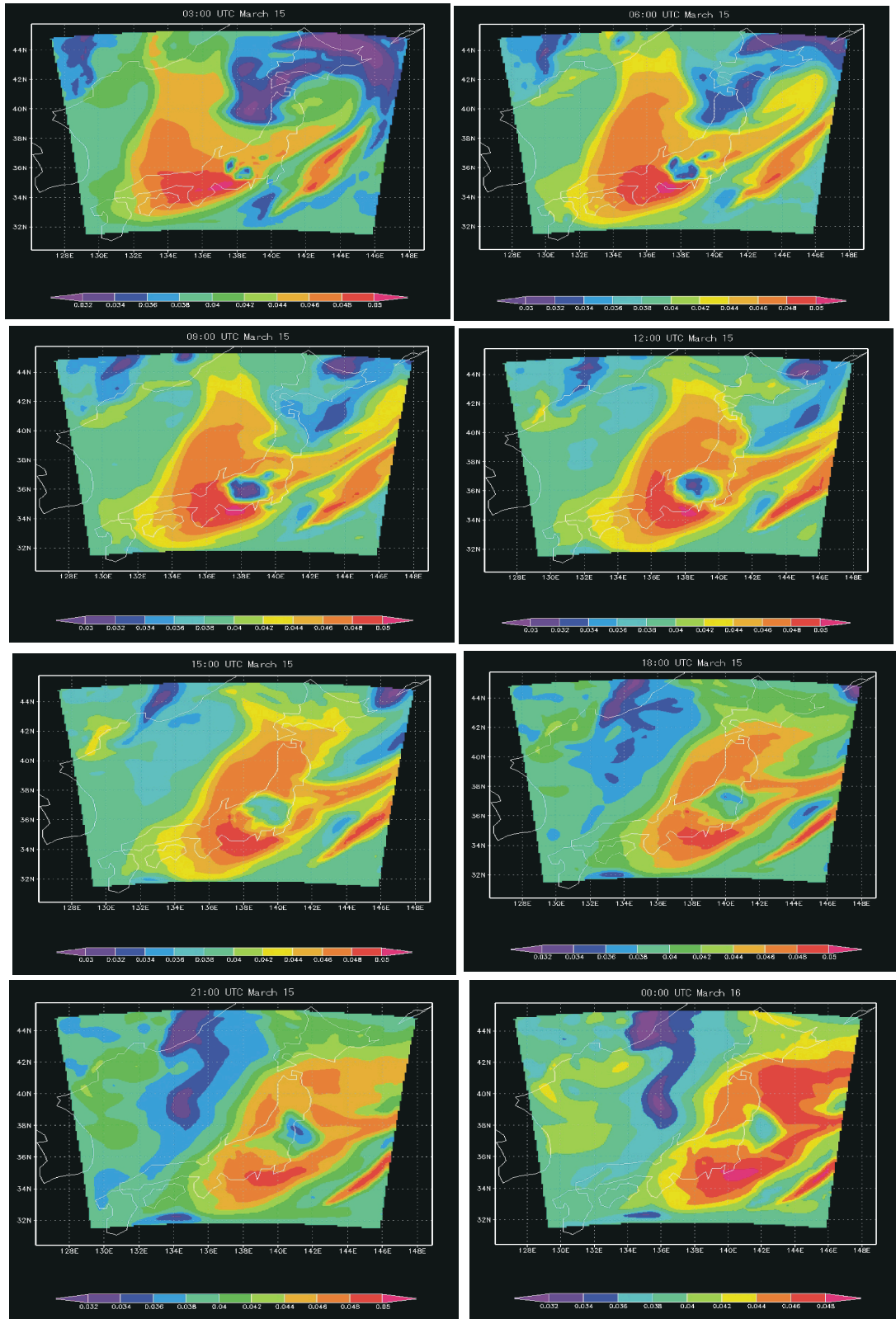


Fig. 4: Ozone concentrations (ppm) over the Sea of Japan coastal area from 00:03 UTC of March 14 to 00:00 UTC of March 16 of the year 2008, which is the simulation result of WRF/Chem model.

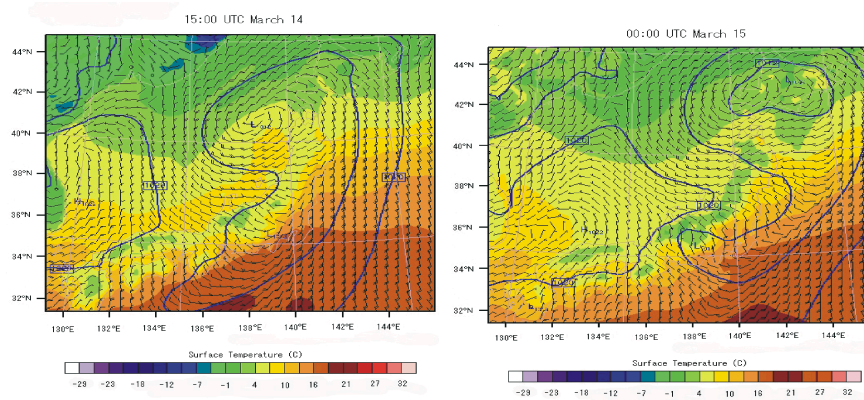


Fig. 5: Temperature distribution ( $^{\circ}\text{C}$ ) in 15:00 UTC of March 14 and 00:00 UTC of March 15.

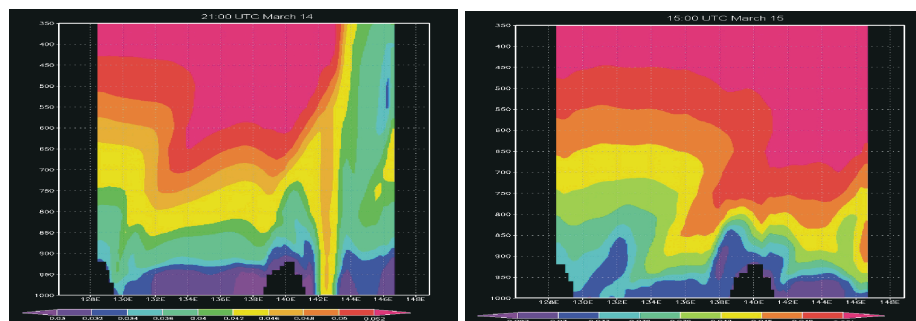


Fig. 6: Vertical distribution of ozone in east west cross-section at fixed latitude 35.7 at 21.00 UTC of March 14 and 15.00 UTC of March 15.

Table 3: Comparison study of average zone concentrations in March between EANET monitoring data and WRF/Chem simulation result.

EANET monitoring stations	EANET monitoring data (ppb)	WRF/Chem simulation result (ppb)
Rishiri	50	42
Tappi	55	44
Ogasawara	46	40
Sado	50	48
Happo	54	46
Ijirako	37.5	44
Oki	47.5	43
Banryuko	44	45
Yasuhara	42.5	43
Hedomisaki	50	40
Populated area	33.5	39

**Local Meteorological Characteristics:** Large-scale winds give the general wind regime and local winds influence the convergence zones. As such, regional circulations play an important role in the dispersion of pollutants [45]. Many studies have showed that wind and weather conditions are one of the most important factors for formation of photochemical pollution. These factors include stable boundary layer, strong solar radiation, clear sky, weak wind, high temperature and low humidity, etc. Figure 5 shows the temporal variations of simulated meteorological conditions of the entire domain. Due to the winter season,

the air temperatures are lower, with daily maximum temperatures are below  $6^{\circ}\text{C}$  (Figure 5) on March and the daily minimum relative humidity was below 75% in general, in which the photochemical pollution was weak. Figure 5 (15:00 UTC of March 14) shows the strong wind in the nighttime in the coastal area of Japan Sea. This illustrates that photochemical reaction may play an important role on the studied episode. It should be noted that the wind speed were relatively strong in the north part of Japan and the temperature was lowered by the influence of the anticyclone, but the  $\text{O}_3$  peaks were

little higher at the south part of Japan (Figure 4), this high O<sub>3</sub> peaks may be mainly attributed to the transport from west to east. Figure 5 shows the magnitude of wind speed and wind direction by WRF simulation. The simulated wind direction shows that Japan was under the control of the westerly or northwesterly winds from the continent [41].

**Vertical Distribution of O<sub>3</sub> Concentrations:** This section analysis the vertical distribution of O<sub>3</sub> concentrations in the PBL and discuss correlations between concentrations at the ground and elevated levels on the vertical sections at a fixed latitude 35.7 between east west cross-section of enter domain at 21.00 UTC of March 14 (6:00 am of March 15 of Japanese Standard Time) and 15.00 UTC of March 15 (12:00 am of March 16 of Japanese Standard Time) respectively. Figure 6 shows the vertical profiles of mean ozone concentrations in the 1.5 km (350 Pa) layer of the atmosphere, based on the WRF/Chem simulation. The vertical concentrations of O<sub>3</sub> were higher in the morning time than that of midnight, while the vertical distribution of tropospheric ozone showed an increase in concentrations with height. It is evident that due to the influence of urbanization in Tokyo metropolitan (latitude 35.7 N, longitude 139.7 E) area the atmospheric boundary layer become quite unstable and thus it is difficult for O<sub>3</sub> to be transported upward and diffused, therefore O<sub>3</sub> was lower in the ground level.

In general, the surface ozone exhibits strong diurnal variation with a mid-afternoon maximum and an early morning minimum [46, 47]. In this study concentrations of ozone in daytime was much larger than those at nighttime (Figure 6). At nighttime, the presence of temperature inversion isolates the surface level ozone from that of upper levels, as there is little or no vertical mixing between the surface layer and levels above the nocturnal boundary layer (NBL). Surface ozone is partly removed by deposition and reaction with nitric oxide (NO). Since no ozone is produced in the absence of sunlight at night, ozone concentrations begin to decrease after sunset, reaching minimum in early morning before sunrise.

After sunrise, the height of the unstable boundary layer begins to increase as the surface is heated and the nocturnal inversion is destroyed. This results in downward mixing of ozone from aloft [48]. Surface ozone is also locally generated by reactions of nitrogen oxides with volatile organic compounds (VOCs) in the presence of sunlight [22, 49, 50]. In this study, ozone concentrations increase rapidly from early

morning to about noon. By noon, the mixing height typically exceeds 1 Km and ozone is well mixed within the mixing layer. Strong photochemical production and strong convection in the mid-afternoon period cause ozone concentrations to reach peak values in the late afternoon. As a result, ozone production decreased with diminishing intensity of sunlight, resulting in a decrease of ozone concentrations with time. At the time of sunset, concentrations decreased substantially below the afternoon maximum value. As a new NBL begun to form in the evening, ozone concentrations near the surface continue to fall due to surface deposition and reaction with NO. Figure 6 shows the typical vertical profile at nighttime was unbalanced caused by dry deposition to the surface and reaction with NO and the typical daytime profile was stable, which reflecting the important roles of both the local production of ozone and greater convective mixing in the vertical.

**Tropospheric Nox Transportation:** Due to anthropogenic activities, the atmospheric trace gas composition has undergone significant changes during the past decades. In particular the tropospheric concentrations of many trace species (e.g. of O<sub>3</sub>, CO, NO, NO<sub>2</sub>, CH<sub>4</sub>) has largely increased. Nitrogen oxides (NO<sub>x</sub> = NO + NO<sub>2</sub>) are key species in atmospheric chemistry and are heavily influenced by anthropogenic emissions. The availability of NO<sub>x</sub> limits photochemical ozone formation in rural and remote regions [22, 51] and particularly in the upper troposphere [52], where the impact of ozone on radiative forcing is strongest [53]. NO<sub>x</sub> also contributes to acid deposition from the atmosphere [54]. While the lifetime of NO<sub>x</sub> in the atmospheric boundary layer (about 1 day) is too short to allow transport over long distances, its lifetime in the upper troposphere is 5 of the order of 5-10 days [55] which is sufficient even for intercontinental transport [56]. However, due to removal processes, transport of reactive nitrogen from the surface, where the largest sources are located, to the upper troposphere is inefficient [57].

In this study, We simulated the evolution of the NO<sub>x</sub> plume with the atmospheric chemical transportation WRF/Chem model. The simulation results show a plume that traveled from East China (06:00 UTC March 14) to eastward over the East Sea, passed the south part of Tohoku region of Japan (00:00 UTC March 15) and then floated towards the Pacific Ocean (00:09 UTC March 15).

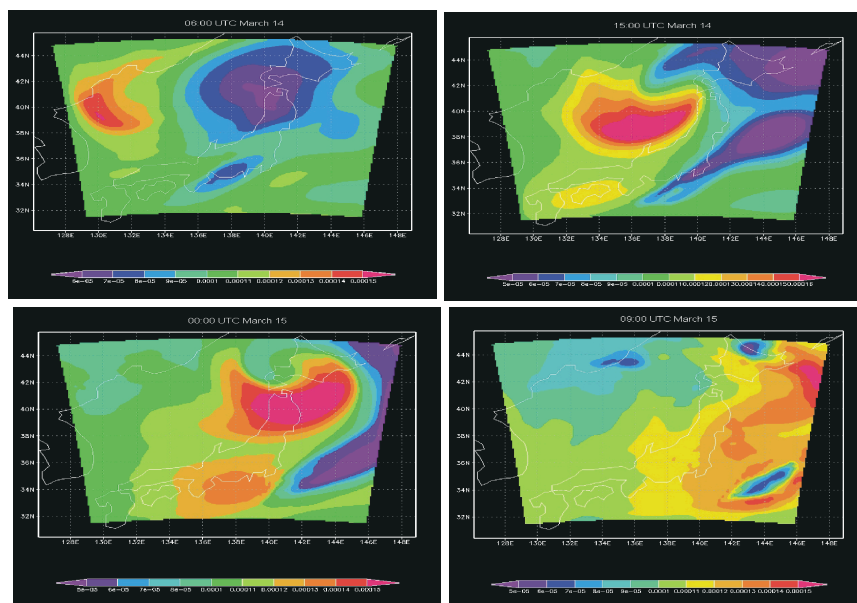


Fig. 7: NOx concentrations ( $\text{g}/\text{m}^3$ ) over the Sea of Japan coastal area.

Figure 7 shows the NOx concentrations ( $\text{g}/\text{m}^3$ ) over the Sea of Japan coastal area. The pink color in the Figure 7 indicates high NOx concentrations ( $150 \mu\text{g}/\text{m}^3$ ) which was formed in East China and driven to eastward by the influence of strong wind. The average range of NOx concentrations in the entire domain was  $70\text{--}120 \mu\text{g}/\text{m}^3$  simulated by WRF/Chem. Since, the photochemical lifetime of NOx depends strongly on presence of  $\text{O}_3$  concentrations through NOx removal reactions, especially conversion to  $\text{N}_2\text{O}_5$  via  $\text{O}_3 + \text{NO}_2 \rightarrow \text{NO}_3 + \text{O}_2$  and  $\text{NO}_2 + \text{NO}_3 \rightarrow \text{N}_2\text{O}_5$ [58], NOx concentration was about  $50\text{--}60 \mu\text{g}/\text{m}^3$  in the purple area of the Figure 7.

## CONCLUSIONS

By using the new generation of regional air quality model WRF/Chem V3.3, a two days heavy-pollution episode in March 2008 was investigated. A rapid  $\text{O}_3$  changes from 00:00 UTC of March 14 to 00:00 UTC of March 16 was observed in the entire domain of the coastal area of the Sea of Japan. During this 2 days period, the daytime and nighttime concentrations of ozone was changed from 50 ppbv to 30 ppbv in the entire domain. In order to understand the processes in controlling this rapid change in  $\text{O}_3$  concentrations, a three dimensional regional chemical/dynamical model (WRF/Chem) is applied to analyze the causes of this rapid  $\text{O}_3$  changes with meteorological conditions. The result shows that the calculated trends of  $\text{O}_3$  concentrations,  $\text{O}_3$  precursors, are

consistent with the measured trends. The calculated magnitudes and diurnal variations of  $\text{O}_3$  are slightly underestimated to the measured results in most of the rural areas, while are overestimated at a urban populated areas, suggesting that the industrial emissions or emission from biomass burning at this sites are significantly underestimated in this study and needs to be improved. Because the model horizontal resolution is  $1^\circ \times 1^\circ$  in this study, the relatively coarse resolution also can lead to the overestimation in  $\text{O}_3$  calculation. Therefore, the resolution of WRF/Chem in this study may not be enough to predict the ozone concentrations situation over Japanese populated areas. Besides, since the model is capable to calculate the rapid  $\text{O}_3$  change, it is suitable to study the causes of the  $\text{O}_3$  change trend. The analysis of model result suggests that weather conditions play important roles in controlling the surface  $\text{O}_3$  in the coastal areas of the Sea of Japan. Under the winter weather system, the high  $\text{O}_3$  concentrations, which were chemically formed in the inland areas, were rapidly transported to the downwind region of the coastal areas, resulting in low  $\text{O}_3$  concentrations in the urbanized region of East Asia. This study illustrates that the WRF/Chem model is a useful tool to study the high variability of  $\text{O}_3$  concentrations. The study of variability of  $\text{O}_3$  has important implication for the prediction of  $\text{O}_3$  concentrations and for the control strategies of high  $\text{O}_3$  events in the coastal areas of the Sea of Japan.

## ACKNOWLEDGEMENTS

We wish to thank Professor Kobayashi Tomonao of the Faculty of Engineering of Gifu University for sharing resources and data with us. The deepest gratitude is also expressed to Naher Meherun the late wife of first author and a former doctoral student of the Graduate School of Agriculture, Gifu University, who passed away in February 2010.

## REFERENCES

1. Molina, L. and M. Molina, (Eds.), 2002. Air Quality in the Mexico MegaCity: An Integrated Assessment. Kluwer Academic Publishers, Dordrecht.
2. Paul, R.A., W.F. Biller and T. McCurdy, 1987. National Estimates of Population Exposure to Ozone. Presented at the Air Pollution Control Association 80th Annual Meeting and Exhibition, New York, NY, USA, pp: 21-26.
3. Tie, X., G. Brasseur, C. Zhao, C. Granier, S. Massie, Y. Qin, P.C. Wang, G.L. Wang and P.C. Yang, 2006. Chemical characterization of air pollution in eastern China and the eastern United States. *Atmospheric Environ.*, 40: 2607-2625.
4. Geng, F.H., C.S. Zhao, X. Tang, G.L. Lu and X. Tie, 2007. Analysis of ozone and VOCs measured in Shanghai: a case study. *Atmospheric Environ.*, 41: 989-1001.
5. Deng, X.J., X. Tie, D. Wu, X.J. Zhou, H.B. Tan, F. Li and C. Jiang, 2008. Long-term trend of visibility and its characterizations in the Pearl River Delta Region (PRD), China. *Atmospheric Environ.*, 42(7): 1424-1435.
6. Zhang, Q., C. Zhao, X. Tie, Q. Wei, G. Li and C. Li, 2006. Characterizations of aerosols over the Beijing region: a case study of aircraft measurements. *Atmospheric Environment*, 40: 4513-4527.
7. Sillman, S., 1995. The use of NO<sub>y</sub>, H<sub>2</sub>O<sub>2</sub> and HNO<sub>3</sub> as indicators for ozone-NO<sub>x</sub>-hydrocarbon sensitivity in urban locations. *J. Geophysical Res.*, 100: 14175-14188.
8. Kleinman, L.I., P.H. Daum, D.G. Imre, J.H. Lee, Y.N. Lee, L.J. Nunnermacker, S.R. Springston, J. Weinstein-Lloyd and L. Newman, 2000. Ozone production in the New York City urban plume. *Journal of Geophysical Research*, 105: 14495-14512. doi:10.1029/2000JD900011.
9. Lei, W. B. De Foy, M. Zavala, R. Volkamer and L.T. Molina, 2007. Characterizing ozone production in the Mexico City Metropolitan area, a case study using a chemical transport model. *Atmospheric Chemistry and Physics*, 7: 1347-1366.
10. Zhang, R., W. Lei, X. Tie and P. Hess, 2004. Industrial emissions cause extreme diurnal urban ozone variability. *Proceedings of the National Academy Science of United States of America*, 101: 6346-6350.
11. Tie, X., S. Madronich, G.H. Li, Z.M. Ying, R. Zhang, A. Garcia, J. Lee-Taylor and Y. Liu, 2007. Characterizations of chemical oxidants in Mexico City: a regional chemical/ dynamical model (WRF/Chem) study. *Atmospheric Environ.*, 41: 1989-2008.
12. Zavala, M., W. Lei, M.J. Molina and L.T. Molina, 2009. Modeled and observed ozone sensitivity to mobile-source emissions in Mexico City. *Atmospheric Chemistry and Physics*, 9: 39-55.
13. Geng, F.H., Z. Qiang, X. Tie, M. Huang, X. Ma, Z. Deng, J. Quan and C. Zhao, 2009. Aircraft measurements of O<sub>3</sub>, NO<sub>x</sub>, CO, VOCs and SO<sub>2</sub> in the Yangtze River Delta region. *Atmospheric Environ.*, 43: 584-593.
14. Stephens, S., S. Madronich, F. Wu, J.B. Olson, R. Ramos, A. Retama and R. Munoz, 2008. Weekly patterns of Mexico City's surface concentrations of CO, NO<sub>x</sub>, PM<sub>10</sub> and O<sub>3</sub> during 1986-2007. *Atmospheric Chemistry and Physics*, 8: 5313-5325.
15. Ying, Z.M., X. Tie and G.H. Li, 2009. Sensitivity of ozone concentrations to diurnal variations of surface emissions in Mexico City: a WRF/Chem modeling study. *Atmospheric Environ.*, 43: 851-859.
16. Kida, M., 2005. Air Quality Management Division, Environmental Bureau, Ministry of the Environment, Japan; Countermeasures on chemical substances in Japan by Air Pollution Control Law. Available from: [http://infofile.pcd.go.th/air/VOC\\_kida.pdf?CFID=1412050&CFTOKEN=60317530](http://infofile.pcd.go.th/air/VOC_kida.pdf?CFID=1412050&CFTOKEN=60317530).
17. United Nations (UN) Statistics Division, 1 April 2010. Standard Country and Area Codes Classifications. Retrieved 16 July 2010. Available from: <http://unstats.un.org/unsd/methods/m49/m49regin.htm#asia>.
18. Finlayson-Pitts B.J. and J.N. Pitts, 2000. Chemistry of the Upper and Lower Atmosphere-Theory, Experiments and Applications. Academic Press, San Diego.

19. Seinfeld, J.H. and S.N. Pandis, 1998. *Atmospheric Chemistry and Physics - from Air Pollution to Climate Change*. John Wiley and Sons, New York.
20. Thielmann, A., A.S.H. Prevot and J. Staehelin, 2002. Sensitivity of ozone production derived from field measurements in the Italian Po basin. *J. Geophysical Res.*, 107: 8194, doi: 10.1029/2000JD000119.
21. Althuller, A.P. and A.S. Lefohn, 1996. Background ozone in the planetary boundary layer over the United States. *J. the Air Waste Management Association*, 46: 134-141.
22. Chameides, W.L., F. Fehsenfeld, M.O. Rodgers, C. Cardelino, J. Martinez, D. Parrish, W. Lonneman, D.R. Lawson, *et al.* 1992. Ozone precursor relationships in the ambient atmosphere. *J. Geophysical Res.*, 97: 6037-6055.
23. NRC (National Research Council), 1991. *Rethinking the Ozone Problem in Urban and Regional Air Pollution*. National Academy Press: Washington DC.
24. U.S. Environmental Protection Agency (U.S. EPA), Office of Air Quality Planning and Standards, 1999. *Guideline for Development an Ozone Forecasting Program*. EPA-454/R-99-009. Available from: <http://www.epa.gov/ttncaaa1/t1/memoranda/foregu id.pdf>.
25. Skamarock, W.C., J.B. Klemp, J. Dudhia, D.O. Gill, D.M. Barker, W. Wang and J.G. Powers, 2005. A Description of the Advanced Research WRF Version 2. NCAR Tech. Note. TN-468tSTR, pp: 88. Available from: [http://www.wrf-model.org/wrfadmin/docs/arw\\_v2.pdf](http://www.wrf-model.org/wrfadmin/docs/arw_v2.pdf).
26. Grell, G.A., S.E. Peckham, R. Schmitz, S.A. McKeen, G. Frost, W. Skamarock and B. Eder, 2005. Fully coupled "online" chemistry within the WRF model. *Atmospheric Environ.*, 39: 6957e6975.
27. Wesley, M.L., 1989. Parameterization of surface resistance to gaseous dry deposition in regional numerical models. *Atmospheric Environ.*, 16: 1293-1304.
28. Madronich, S. and S. Flocke, 1999. The role of solar radiation in atmospheric chemistry. *Handbook of Environmental Chemistry* (P. Boule, ed.), Springer-Verlag, Heidelberg, pp: 1-26.
29. Tie, X., X. S. Madronich, S. Walters, R. Zhang, P. Rasch and W. Collins, 2003. Effect of clouds on photolysis and oxidants in the troposphere. *Journal of Geophysical Research*, 108(D20): 4642, doi:10.1029/2003JD003659.
30. Chang, J.S., F.S. Binkowski, N.L. Seaman, J.N. McHenry, P.J. Samson, W.R. Stockwell, C.J. Walcek, S. Madronich, P.B. Middleton, J.E. Pleim and H.H. Lansford, 1989. The regional acid deposition model and engineering model. *State-of-Science/Technology, Report 4*, National Acid Precipitation Assessment Program, Washington, DC.
31. Schell, B., I.J. Ackermann, H. Hass, F.S. Binkowski and A. Ebel, 2001. Modeling the formation of secondary organic aerosol within a comprehensive air quality model system. *J. Geophysical Res.*, 106: 28275-28293.
32. BBC News, S Korea bid to solve sea dispute, 2007-01-08. Retrieved on 2008-02-17. South Korea calls it the East Sea. Available from: <http://news.bbc.co.uk/2/hi/asia-pacific/6240051.stm>.
33. Ministry of Foreign Affairs and Trade (MFAT) of South Korea, 2007. Report on the Progress in Consultations on the Naming of the Sea Area between the Korean Peninsula and the Japanese Archipelago. Retrieved on 2008-02-17. The sea area has been consistently called "East Sea" in Korea. Available from: <http://www.mofat.go.kr/press/hotissue/eastsea/res /EastSea1.doc>.
34. David, W.A., N. Ashby and C.C. Hodge, 1997. *The Science of Timekeeping*. Hewlett-Packard. Application Note 1289. Available from: [http://www.allanstime.com/Publications/DWA/Science\\_Timekeeping/TheScienceOfTimekeeping.pdf](http://www.allanstime.com/Publications/DWA/Science_Timekeeping/TheScienceOfTimekeeping.pdf).
35. Hanado, Y., K. Imamura, N. Kotake, F. Nakagawa, Y. Shimizu, R. Tabuchi, Y. Takahashi, M. Hosokawa, T. Morikawa, 2008. The new Generation System of Japan Standard Time at NICT. *International J. Navigation and Observation*, ID841672.
36. Binkowski, F.S. and U. Shankar, 1995. The regional particulate matter model, 1. Mode description and preliminary results. *J. Geophysical Res.*, 100: 26191-26209.
37. Japan Meteorological Agency (JMA). Annual Report on Atmospheric and Marine Environment Monitoring. Observation Results for 2008. Available from: [http://www.data.kishou.go.jp/obs-env/cdrom/report2008/html/figures\\_e.html](http://www.data.kishou.go.jp/obs-env/cdrom/report2008/html/figures_e.html).
38. Japan Meteorological Agency (JMA). Annual Report on Atmospheric and Marine Environment Monitoring, No. 11. Observation Results for 2009. Available from: <http://www.data.kishou.go.jp/obs-env/cdrom/report/pdf/booklet.pdf>.

39. National Institute for Environmental Studies, 2010. Observation data are available from: [http://www.nies.go.jp/igreen/td\\_down.html](http://www.nies.go.jp/igreen/td_down.html) (in Japanese).
40. Ministry of the Environment (MOE), 2010. Observation data are available from: <http://www.env.go.jp/air/osen/index.html> (in Japanese), last access: 20 August 2010.
41. Chatani, S. and K. Sudo, 2011. Influences of the variation in inflow to East Asia on surface ozone over Japan during 1996-2005. *Atmospheric Chemistry and Physics*, 11: 8745-8758.
42. Val, B., 2008. Cyclones and Anticyclones in the Mid-Latitudes. power point presentation. Accessed from: [http://www.google.com/url?sa=t&rc=tj&q=&esrc=s&frm=1&source=web&cd=4&ved=OCC8QFjAD&url=http%3A%2F%2Fwww.aos.wisc.edu%2F~aos101vb%2Fval\\_cyclones.ppt&ei=mJrHTpTSJKjMmA XerdEQ&usg=AFQjCNHHJiyzhD760\\_M\\_a99qE8cvt9Hp6A&sig2=PUTZj7KcWwb32iMN7tpNaQ](http://www.google.com/url?sa=t&rc=tj&q=&esrc=s&frm=1&source=web&cd=4&ved=OCC8QFjAD&url=http%3A%2F%2Fwww.aos.wisc.edu%2F~aos101vb%2Fval_cyclones.ppt&ei=mJrHTpTSJKjMmA XerdEQ&usg=AFQjCNHHJiyzhD760_M_a99qE8cvt9Hp6A&sig2=PUTZj7KcWwb32iMN7tpNaQ).
43. Jet Stream: An Online School For Weather, 2008. The Sea Breeze. National Weather Service. Accessed October 24, 2006. Available from: <http://www.srh.weather.gov/srh/jetstream/index.htm>.
44. Vautard, R., C. Honore, M. Beekmanna and L. Rouil, 2005. Simulation of ozone during the August 2003 heat wave and emission control scenarios. *Atmospheric Environ.*, 39: 2957-2967.
45. Seaman, N.L., 2000. Meteorological modeling for air-quality assessments. *Atmospheric Environment*, 34: 2231-2259.
46. Logan, J.A., 1989. Ozone in rural areas of the United States. *J. Geophysical Res.*, 94: 8511-8532.
47. Parrish, D.D., M.P. Buhr, M. Trainer, *et al.* 1993. The total oxidized nitrogen levels and the partitioning between the individual species at six rural sites in eastern North America. *J. Geophysical Res.*, 98: 2927-2939.
48. Trainer, M., E.J. Williams, D.D. Parrish, M.P. Buhr, E.J. Allwine, H.H. Westberg, F.C. Fehsenfeld and S.C. Liu, 1987. Models and observations of the impact of natural hydrocarbons on rural ozone. *Nature*, 329: 705-707.
49. Warneck, P., 1988. *Chemistry of the Natural Atmosphere*. Academic Press Inc. London, UK, pp: 41.
50. NRC (National Research Council), 1992. *Rethinking the Ozone Problem in Urban and Regional Air Pollution*. National Academy Press: Washington DC.
51. Lin, X., M. Trainer and S.C. Liu, 1988. On the nonlinearity of the tropospheric ozone production, *J. Geophysical Res.*, 93: 15879-15888.
52. Levy, H., W.J. Moxim, A.A. Klonecki and P.S. Kasibhatla, 1999. Simulated tropospheric NO<sub>x</sub>: Its evaluation, global distribution and individual source contributions. *J. Geophysical Res.*, 104: 26279-26306.
53. Johnson, C., J. Henshaw and G. McInnes, 1992. Impact of aircraft and surface emissions of nitrogen oxides on tropospheric ozone and global warming. *Nature*, 355: 69-71.
54. Stoddard, J.L., D.S. Jeffries, A. Lukeville, T.A. Clair, P.J. Dillon, C.T. Driscoll, M. Forsius, M. Johannessen, J.S. Kahl, J.H. Kellogg, A. Kemp, J. Mannio, D.T. Monteith, P.S. Murdoch, S.A. Patrick, *et al.* 1999. Regional trends in aquatic recovery from acidification in North America and Europe. *Nature*, 401: 575-578.
55. Jaegle, L., D.J. Jacob, Y. Wang, A.J. Weinheimer, B.A. Ridley, T.L. Campos, G.W. Sachse and D.E. Hagen, 1998. Sources and chemistry of NO<sub>x</sub> in the upper troposphere over the United States. *Geophysical Research Letters*, 25: 1705-1708.
56. Stohl, A., S. Eckhardt, C. Forster, P. James and N. Spichtinger, 2002. On the pathways and timescales of intercontinental air pollution transport. *Journal of Geophysical Research*, 107: 4684, doi: 10.1029/2001JD001396.
57. Murphy, D., D. Fahey, M. Profitt, S. Liu, K. Chan, C. Eubank, S. Kawa and K. Kelly, 1993. Reactive nitrogen and its correlation with ozone in the lower stratosphere and upper troposphere. *J. Geophysical Res.*, 98: 8751-8773.
58. Von Kuhlmann, R., M.G. Lawrence, P.J. Crutzen and P.J. Rasch, 2003. A model for studies of tropospheric ozone and nonmethane hydrocarbons: model description and ozone results. *Journal of Geophysical Res.*, 108(D9): 4294, (doi:10.1029/2002JD002893).
59. Hong, S.Y., J. Dudhia and S.H. Chen, 2004. A Revised Approach to Ice Microphysical Processes for the Bulk Parameterization of Clouds and Precipitation. *Journal of American Meteorological Society*, 132(1): 103-120. Available from: <http://www.mmm.ucar.edu/wrf/users/docs/hongeta104.pdf>.

60. Ahmad, N. and J. Linderman, 2008. A Godunov-type Finite Volume Scheme for Meso- and Micro-scale Flows in Three Dimensions. *Pure and Applied Geophysics*, 165: 1929-1939.
61. Baldauf, M. and W.C. Skamarock, 2009. An improved third order vertical advection scheme for the Runge-Kutta dynamical core. 8th International SRNWP-Workshop on Non-Hydrostatic Modelling. Available from: <http://www.dwd.de/modellierung>.
62. Mlawer, E.J., S.J. Taubman, P.D. Brown, M.J. Iacono and S.A. Clough, 1997. Radiative transfer for inhomogeneous atmosphere: RRTM, a validated correlated-k model for the long wave. *J. Geophysical Res.*, 102D: 16663-16682.
63. Shin, H.H., S.Y. Hong, J. Dudhia and Y.J. Kim, 2010. Orography-Induced Gravity Wave Drag Parameterization in the Global WRF: Implementation and Sensitivity to Shortwave Radiation Schemes. *Advances in Meteorology*, 2010: 8 pages, Article ID 959014, doi:10.1155/2010/959014.
64. Dudhia, J., 1989. Numerical study of convection observed during the winter monsoon experiment using a mesoscale two-dimensional model. *Journal of Atmospheric Sci.*, 46: 3077-3107.
65. Monin, A.S. and A.M. Obukhov, 1954. Basic laws of turbulent mixing in the surface layer of the atmosphere. *Contributions of the Geophysical Institute of the Slovak Academy of Science, USSR*, 151: 163-187 (in Russian).
66. Ek, M.B., K.E. Mitchell, Y. Lin, E. Rogers, P. Grunmann, V. Koren, G. Gayno and J.D. Tarpley, 2003. Implementation of Noah land surface model advances in the National Centers for Environmental Prediction operational mesoscale Eta model. *J. Geophysical Res.*, 108: 8851-67.
67. Janjic, Z.I., 1990. The step-mountain coordinate: Physical package. *Monthly Weather Review*, 118: 1429-1443.
68. Janjic, Z.I., 1994. The step-mountain eta coordinate model: Further development of the convection, viscous sub-layer and turbulent closure schemes. *Monthly Weather Review*, 122: 927-945.
69. Grell, G.A. and D. Devenyi, 2002. A generalized approach to parameterizing convection combining ensemble and data assimilation techniques. *Geophysical Research Letters*, 29, NO 14. 10.1029/2002GL015311, 2002.
70. Stockwell, W.R., P. Middleton and J.S. Chang, 1990. The second generation regional acid deposition model chemical mechanism for regional air quality modeling *J. Geophysical Res.*, 95(D10): 16343-16367.
71. Wesley, M.L., 1989. Parameterization of surface resistance to gaseous dry deposition in regional numerical models. *Atmospheric Environment*, 16: 1293-1304.
72. Guenther, A.B., P.R. Zimmerman, P.C. Harley, R.K. Monson and R. Fall, 1993. Isoprene and monoterpene emission rate variability: model evaluations and sensitivity analyses. *J. Geophysical Research Atmosphere* 98D, 12609e12617.
73. Guenther, A., P. Zimmerman and M. Wildermuth, 1994. Natural volatile organic compound emission rate estimates for US woodland landscapes. *Atmospheric Environ.*, 28: 1197-1210.
74. Madronich, S., 1987. Photodissociation in the atmosphere, 1, actinic flux and the effects of ground reflections and clouds. *J. Geophysical Res.*, 92: 9740-9752.
75. Schell, B., I.J. Ackermann, H. Hass, F.S. Binkowski and A. Ebel, 2001. Modeling the formation of secondary organic aerosol within a comprehensive air quality model system. *J. Geophysical Res.*, 106: 28275-28293.
76. Granier, C., U. Niemeir, J.F. Muller, J. Olivier, J. Peters, A. Richter, H. Nuss, J. Burrows and J. POET POET, 2003. Variation of the atmospheric composition over the 1990-2000 period. Report #6, EU project EVK2-1999-00011.
77. Olivier, J., J. Peters, C. Granier, G. Petron, J.F. Muller and S. Wallens, POET POET, 2003. Present and future surface emissions of atmospheric compounds. Report #2, EU project EVK2-1999-00011.
78. Schultz, M. and RETRO team, 2005. RETRO emission trends and variability. Poster presentation at 1st ACCENT Symposium, Urbino, pp: 12-16.
79. Olivier, J.G.J., A.F. Bouwman, C.W.M. Van der Maas, *et al.* 1996. Description of EDGAR Version 2.0, A set of global emission inventories of greenhouse gases and ozone-depleting substances for all anthropogenic and mos-natural sources on a per country basis and on a 1° x 1° grid. RIVM/TNO representative, RIVM, Bilthoven, number nr. 711060 002, 1006.
80. Olivier, J.G.J., J.P.J. Bloos, J.J.M. Berdowski, A.J.H. Visschedijk and A.F. Bouwman, 1999. A 1990 global emission inventory of anthropogenic sources of carbon monoxide on 1° x 1° developed in the framework of EDGAR/GEIA. *Chemosphere. Global Change Sci.*, 1: 1-17.

81. Olivier, J.G.J., J.J.M. Berdowski, J.A.H.W. Peters, J. Bakker, A.J.H. Visschedijk and J.P.J. Bloos, 2001. Applications of EDGAR. Including a description of EDGAR 3.0: reference database with trend data for 1970-1995. RIVM, Bilthoven. RIVM report no. 773301 001/ NOP report no. 410200 051.
82. Van der Werf, G.R., J.T. Randerson, G.J. Collatz, L. Giglio, P.S. Kasibhatla, A. Avelino, S.C. Olsen and E.S. Kasischke, 2004. Continental-scale partitioning of fire emissions during the 1997-2001 El Nino / La Nina period. *Science*, 303: 73-76.
83. Van der Werf, G.R.J., T. Randerson, L. Giglio, G.J. Collatz and P.S. Kasibhatla, 2006. Interannual variability in global biomass burning emission from 1997 to 2004. *Atmospheric Chemistry and Physics*, 6: 3423-3441. SRef-ID: 1680-7324/acp/2006-6-3423.
84. Andres, R.J., D.J. Fielding, G. Marland, T.A. Boden and N. Kumar, 1999. Carbon dioxide emissions from fossil-fuel use 1751-1950. *Tellus 51B*: 759-65.